Temporal variability of the carbonate system and air-sea CO 2 exchanges in a Mediterranean human-impacted coastal site

Cathy Wimart-Rousseau, Katixa Lajaunie-Salla, Pierre Marrec, Thibaut Wagener, Patrick Raimbault, Véronique Lagadec, Michel Lafont, Nicole Garcia, Frédéric Diaz, Christel Pinazo, et al.

Contents lists available at ScienceDirect

Estuarine, Coastal and Shelf Science

journal homepage: http://ees.elsevier.com

Temporal variability of the carbonate system and air-sea CO_2 exchanges in a Mediterranean human-impacted coastal site

Cathy Wimart-Rousseau [a,*], Katixa Lajaunie-Salla [a], Pierre Marrec [f], Thibaut Wagener [a,**], Patrick Raimbault [a], Véronique Lagadec [a], Michel Lafont [a], Nicole Garcia [a], Frédéric Diaz [a], Christel Pinazo [a], Christophe Yohia [d], Fabrice Garcia [a], Irène Xueref-Remy [b], Pierre-Eric Blanc [c], Alexandre Armengaud [e], Dominique Lefèvre [a,***]

[a] Aix Marseille Univ, Université de Toulon, CNRS, IRD, MIO, UM 110, 13288, Marseille, France
[b] Aix Marseille Univ, Avignon Université, CNRS, IRD, Institut Méditerranéen de Biodiversité et d'Ecologie Marine et Continentale (IMBE), Marseille, France
[c] Observatoire de Haute Provence, OSU Pythéas, France
[d] Aix Marseille Univ., Université de Toulon, CNRS, IRD, OSU Institut Pythéas, 13288, Marseille, France
[e] AtmoSud: Observatoire de la Qualité de l'air en Région Sud Provence Alpes Côte d'Azur, le Noilly Paradis, 146 Rue Paradis, 13294, Marseille, Cedex 06, France
[f] University of Rhode Island, Graduate School of Oceanography, Menden-Deuer Lab, Narragansett, RI, 02882, USA

ARTICLE INFO

Keywords
Coastal biogeochemistry
CO_2 fluxes
Carbonate system
North Western Mediterranean Sea
Bay of Marseille

ABSTRACT

The temporal evolution of the carbonate system and air-sea CO_2 fluxes are investigated for the first time in the Bay of Marseille (BoM – North Western Mediterranean Sea), a coastal system affected by anthropogenic forcing from the Marseille metropolis. This study presents a two-year time-series (between 2016 and 2018) of fortnightly measurements of A_T, C_T, pH and derived seawater carbonate parameters at the SOLEMIO station. On this land-ocean boundary area, no linear relationship between A_T and salinity in surface water is observed due to sporadic intrusions of freshwater coming from the Rhone River. On an annual scale, the BoM acts as a sink of atmospheric CO_2. This result is consistent with previous studies in the Mediterranean Sea. Mean daily air-sea CO_2 fluxes range between −0.8 mmol C.m^{-2}.d^{-1} and -2.2 mmol C.m^{-2}.d^{-1} during the study period, depending on the atmospheric CO_2 sampling site used for the estimates. This study shows that the pCO_2 in the surface water is predominantly driven by temperature changes, even if partially counterbalanced by biological activity. Therefore, temperature is the main contributor to the air-sea CO_2 exchange variability. Mean daily Net Ecosystem Production (NEP) estimates from C_T budget shows an ecosystem in which autotrophic processes are associated with a sink of CO_2. Despite some negative NEP values, the observed air-sea CO_2 fluxes in the BoM are negative, suggesting that thermodynamic processes are the predominant drivers for these fluxes.

1. Introduction

Since the beginning of the industrial era, human activities have resulted in an increase in carbon dioxide (CO_2) emissions into the atmosphere. The global annual average atmospheric CO_2 concentration of 405 ppm was reached in 2017 (Dlugokencky and Tans, 2019). This increase in CO_2 is likely to be the main factor responsible for current climate change (IPCC, 2018). The ocean plays a major role in mitigating climate change via the CO_2 exchanges at the air-sea interface and sequestration into deep water. Between 1994 and 2007, 2.6 ± 0.3 PgC.a^{-1} of CO_2 was absorbed annually (Gruber et al., 2019), representing 31 ± 4% of the global anthropogenic CO_2 emissions. This absorption of CO_2 by seawater induces an increase in hydronium ion concentration (*i.e.* a decrease in the pH of seawater). As seawater becomes more acidic, it causes carbonate ions to be relatively less abundant, which has a significant impact on biological and physio-chemical processes (Doney et al., 2009). This process is called "ocean acidification". Carbon budgets in near-shore areas such as seagrass beds (Huang et al., 2015; Kirkman and Reid, 1979) and coral reefs (Suzuki and Kawahata, 2003; Ware et al., 1992) are well documented, but coastal oceanic areas that cover about 7% of the oceanic domain (Wollast, 1998) are usually neglected when producing global carbon budgets. However, recent studies have highlighted that coastal seas act as a sink of CO_2 with a range of between 0.2 and 0.4 PgC.a^{-1} (Borges et al., 2006), with a recent regionalised global CO_2 sink estimate of 0.19 ± 0.05 PgC.a^{-1} (Laruelle et al., 2014), that is between 8% and 15% of the oceanic CO_2 sink. Although open-ocean CO_2 inventories and dynamics have been studied in detail over the last 30 years (Gruber et al., 2019; Takahashi et al., 2002), the importance of coastal oceanic areas has been underestimated (Bourgeois et al., 2016; Gattuso et al., 1998). In contrast to open-ocean acidification trends ranging from

* Corresponding author.
** Corresponding author.
*** Corresponding author.
E-mail addresses: cathy.wimart-rousseau@mio.osupytheas.fr (C. Wimart-Rousseau); thibaut.wagener@mio.osupytheas.fr (T. Wagener); dominique.lefevre@mio.osupytheas.fr (D. Lefèvre)

https://doi.org/10.1016/j.ecss.2020.106641
Received 5 June 2019; Received in revised form 13 January 2020; Accepted 10 February 2020

−0.0004 (Astor et al., 2013) to −0.0026 pH units.a^{-1} (Olafsson et al., 2010), rates of change in pH of coastal systems range from −0.023 to 0.023 pH units.a^{-1} (Carstensen and Duarte, 2019). Coastal areas are under the influence of multiple and diverse forcing variables due to their interactions with the land and human activities (Borges et al., 2006; Bourgeois et al., 2016).

The Mediterranean Sea (MedSea) more specifically is subjected to significant land-ocean interactions along its coastal areas. Because of its semi-enclosed nature and smaller inertia, due to the relatively short residence time of its water masses, it is highly reactive to external forcing variables in particular variations in water, energy and matter fluxes at the interfaces (Durrieu de Madron et al., 2011). The role of the MedSea as a source or sink for atmospheric CO_2 in the global carbon cycle, especially in the context of warming MedSea waters, is unclear (Nykjaer, 2009; Vargas-Yáñez et al., 2008). Several recent studies indicate a gradual change from a source to a sink over the last few decades (Louanchi et al., 2009; Taillandier et al., 2012). However, *in situ* measurements of the carbonate seawater system are still scarce for the MedSea. In recent years, a few cruises have given a clearer description of the carbonate system at the basin scale (Álvarez et al., 2014). For the North Western (NW) part of the basin, time-series of carbonate chemistry exist in the Ligurian Sea at the DYFAMED and ANTARES sites (Fig. 1 – *e.g.*, Copin-Montégut and Bégovic, 2002; Coppola et al., 2018; Hood and Merlivat, 2001; Lefèvre, 2010; Merlivat et al., 2018; Touratier and Goyet, 2009), in the Bay of Villefranche-sur-Mer at the Point B station (Fig. 1 - De Carlo et al., 2013; Kapsenberg et al., 2017) and in the Gulf of Trieste at the coastal C1 station (Ingrosso et al., 2016).

The Bay of Marseille (BoM) is located in the NW MedSea on the Gulf of Lions continental shelf and is adjacent to the metropolis of Marseille, the second biggest city in France (Fig. 1) with a population of over 1 million inhabitants. Due to this proximity, the BoM sporadically receives (especially during flood events) effluents from the sewage system and coastal rivers enriched in nutrients, organic matter and chemical products (Millet et al., 2018). The bay also experiences strong winds (Petrenko, 2003) and large seasonal temperature variations (http://somlit.oasu.u-bordeaux.fr/mysomlit-public/). Northern Current intrusions (Petrenko, 2003) also contribute to a non-negligible influence on the shelf circulation.

Finally, in addition to these complex dynamics, under specific conditions, water masses in the BoM can be influenced by the extension to the East of the Rhone River plume (Fraysse et al., 2014; Gatti et al., 2006), even though the Rhone River estuary is 35 km West of the BoM and does not flowing directly into the BoM. The Rhone River is the major input of freshwater into the Western MedSea with a mean annual discharge of 1700 m^3 s^{-1} which can reach more than 11 200 m^3 s^{-1} during centennial flooding (Pont et al., 2002).

In consequence, the ecosystem of the BoM is subject to large daily and seasonal variability in the physical and chemical forcing. These will directly affect biological processes such as photosynthesis, respiration or $CaCO_3$ precipitation and dissolution (Bensoussan and Gattuso, 2007). Moreover, due to the nearby highly urbanised area, high atmospheric CO_2 concentrations (up to 540 ppm) with large daily variability have been observed and may directly affect seawater pCO_2.

The SOLEMIO station located in the BoM (Fig. 1) is part of the French national network of coastal observation SOMLIT (Service d'Observation en Milieu LITtoral – http://somlit.epoc.u-bordeaux1.fr/fr/). This network was implemented in 1994 for the monitoring of physical, chemical and biological parameters. Within this network, core parameters are collected in order to address the long-term evolution of coastal ecosystems. Measurements of carbonate chemistry parameters are not routinely measured within the framework of the SOMLIT network.

This paper presents a two-year time-series of carbonate chemistry data acquired between June 2016 and July 2018 in the BoM at SOLEMIO with the aim of deciphering the main physical and biological processes driving this carbonate system time-series. In light of the current knowledge concerning carbonate chemistry in the MedSea, the results will (1) study the seasonality of the carbonate system and highlight the impact events in the bay, (2) evaluate the CO_2 exchanges between this coastal system and the atmosphere and (3) estimate, with

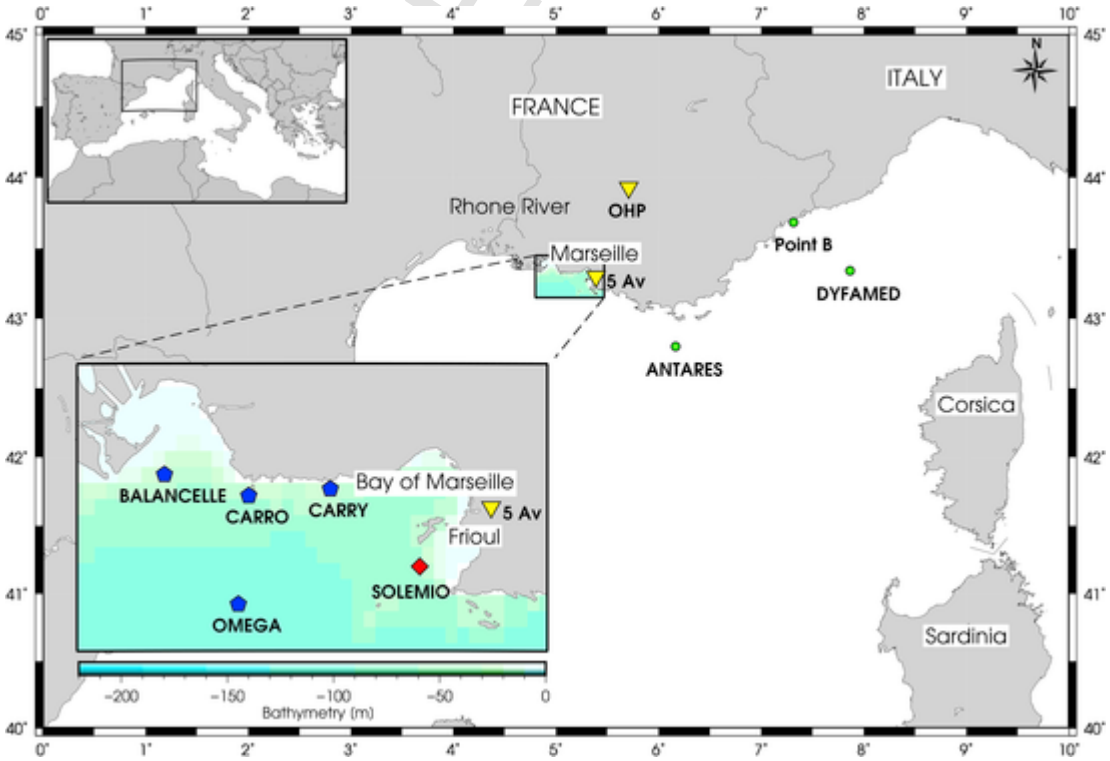

Fig. 1. The area of the North Western Mediterranean Sea showing the Southern coast of France, Corsica and Sardinia, the location of the DYFAMED (43°25′N – 7°52′E), Point B (43°41.10′N – 7.18.94′E) and the ANTARES (42°50′N – 6°10′E) study sites, the SOLEMIO station (43°14.30′N – 5°17.30′E) and the STPS network with its four buoys: the Balancelle buoy (43°20.443′N – 4°55.464′E), the Omega buoy (43°11.952′N – 5°01.789′E), the Carro buoy (43°18.716′N – 5°09.641′E) and the Carry buoy (43°19.146′N – 5°09.641′E). The OHP (43°55.9′N – 5°42.8′E) and 5 Av (43°18.4′N – 5°23.7′E) are the sites that measure atmospheric CO_2. The bathymetry of the area is in meters.

numerous assumptions, the importance of biological processes on CO_2 exchanges in the BoM. The limitations highlighted in this study will support the discussion for recommending future studies in this dynamic coastal ecosystem.

2. Methods

2.1. Sampling strategy and oceanic data acquisition

Sampling and measurements were carried out fortnightly at the SOLEMIO station in the NW MedSea (43°14.10′N – 5°17.30′E, 55 m bottom depth; Fig. 1) from the R.V. Antedon II from June 6th, 2016 to July 11th, 2018. Physical properties of the water column (temperature, conductivity, depth) were measured *in situ* with a SeaBird 9 or a SeaBird 19+ profiler. Sensors were calibrated at least every 2 years (last calibration in January 2017). Conductivity (SBE4 sensor, Seabird®) and temperature (SBE3 sensor, Seabird®) measurements were recorded with a precision of 0.0003 S m^{-1} and 0.001 °C, respectively. Calibration reports indicate a mean annual drift for the temperature and conductivity sensors of ±0.001 °C and of ±0.002 S m^{-1}, respectively. Salinity is expressed using the Practical Salinity Scale. Data is reported as mean ± standard deviation.

Discrete water samples were collected at 3 depths (surface layer, intermediate layer and bottom layer), using 12 dm^3 Niskin® bottles attached to the rosette. Only discrete water samples collected at 2 depths (1 m and 55 m) were used.

2.2. Sample analysis

Samples for dissolved inorganic carbon (C_T) and total alkalinity (A_T) were collected into acid washed 500 cm^3 borosilicate glass bottles and poisoned with 200 mm^3 of a 36 g m^{-3} $HgCl_2$, as recommended by Dickson, 2007. Samples were stored in the dark at 4 °C for 1–6 months before analysis. Measurements of C_T and A_T were performed simultaneously by potentiometric acid titration using a closed cell following the methods described by Edmond (1970) and Dickson and Goyet, 1994. Analyses were performed at the National facility for analysis of carbonate system parameters (SNAPO-CO_2, LOCEAN, Sorbonne University – CNRS, France) with a prototype developed at LOCEAN. Average accuracy of A_T and C_T analysis was 2.3 and 2.6 μmol kg^{-1}, respectively, validated using Certified Reference Material (CRM) provided by A. Dickson's laboratory (Scripps Institution of Oceanography, San Diego).

The pH was measured spectrophotometrically at the MIO (Mediterranean Institute of Oceanography, Marseille – France). Unpurified m-cresol purple (McP) dye (Sigma®) at standard temperature (25 °C) was used and results are reported on the total hydrogen ion concentration scale (pH_T). Measurements were performed following the protocol described by Clayton and Byrne (1993) based on the dissociation of the pH-sensitive indicator dye in the water sample. Within the pH-range of seawater, the dye dissociates into a protonated and an unprotonated form which have different absorbance spectra in the visible range. The ratio of absorbance between 578 and 434 nm was used to determine seawater pH. The parameter pH_T was calculated following Dickson, 2007. The reproducibility of the measurements based on replicates measurements was 0.001 (mean value = 8.047, n = 8).

Unfiltered samples were collected for nutrient analysis in 60 cm^3 polyethylene flasks and immediately frozen. Nutrient concentrations were obtained following the protocol of Aminot and Kérouel (2007). Detection limits for nitrite (NO_2^-), nitrate (NO_3^-), and silicate ($Si(OH)_4$) were of 0.05 μM and 0.003–0.006 μM for phosphate (PO_4^{3-}); the relative precision of these analyses ranged from 5% to 10% (Aminot and Kérouel, 2007). Analysis of nutrients follows the protocols and the quality assurance process set by the SOMLIT network (http://somlit.epoc.u-bordeaux1.fr).

Over these two-years of sampling, 140 samples distributed over the 3 depths of the water column (surface layer, intermediate layer and bottom layer) were obtained.

2.3. Ancillary data

Average weekly wind speeds at 10 m altitude above the water surface (U_{10}, in $m.s^{-1}$) and daily precipitation at the SOMLIT site were obtained from the WRF (Weather Research Forecast) model (gridded by 2 × 2 km). Total atmospheric pressure (P_T, in atm) was obtained from the Meteo France station (WMS07650) at the Marseille-Marignane Airport (43°26.4′N – 5°13.8′E). Atmospheric CO_2 data (mole fraction of CO_2 in dry air in ppm, $[CO_2]_{atm}$) from the OHP site (43°55.9′N – 5°42.8′E; Observatoire de Haute Provence, ST Michel l'Observatoire – France) and 5 Av site (43°18.4′ N – 5°23.7′E; Cinq Avenues, Marseille – France; Fig. 1) were retrieved from the ICOS National Network, France (http://www.obs-hp.fr/ICOS/Plaquette-ICOS-201407_lite.pdf) and the AtmoSud Regional Atmospheric Survey Network, France (https://www.atmosud.org), respectively. The conversion of $[CO_2{}^{atm}]$ (mole fraction of CO_2 in ppm) into pCO_2 (partial pressure of CO_2) was done according to equation (1):

$$pCO_2{}^{A_{TM}} = [P_T - (H/100) \times P_{H2O}] \times [CO_2{}^{atm}] \quad (1)$$

where $pCO_2{}^{A_{TM}}$ is the atmospheric partial pressure of CO_2 (in μatm), P_T is the total atmospheric pressure in atm), H is the relative humidity (here 100%) and P_{H2O} is the vapour pressure of water at ambient temperature (in atm). P_{H2O} was determined from surface seawater temperature (Dean and Lange, 1999). The estimated total error of the atmospheric pCO_2 calculated is 2 μatm.

A network composed of 4 STPS probes (Salinity, Temperature and Pressure Sensors, NKE®) was installed onto sub-surface buoys (the Balancelle, Carro, Carry and Omega buoys) along the coast between the mouth of the Rhone River and the BoM. This network follows and identifies discharges from the Rhone River by measuring hourly temperature and salinity data. The SOLEMIO site (Fig. 1) completes this network inside the BoM.

2.4. Derived data

2.4.1. Mixed layer depth

In this study, the mixed layer depth (MLD) is defined as the depth where the temperature is 0.5 °C lower than the sea surface (1 m) temperature (Monterey and Levitus, 1997). Vertical profiles of temperature in the water column from the CTD were used to estimate the MLD.

2.4.2. Carbonate system parameters

Derived seawater carbonate system parameters (seawater partial pressure of CO_2 ($pCO_2{}^{SW}$) and saturation states for calcite and aragonite) were estimated from A_T and C_T values. Calculations were made with the software program CO2SYS (version 2.1) (Pierrot et al., 2006), considering silicate and phosphate concentrations. As recommended by Álvarez et al. (2014) for the MedSea, the carbonic acid dissociation constants *K*1 and *K*2 from Mehrbach el al. (1973) as refitted by Dickson and Millero (1987) and the dissociation constant for HSO_4^- form Dickson (1990) were used.

Although the pH-C_T couple gives more accurate estimations for seawater pCO_2 (Millero, 1995), A_T and C_T values were used. This choice was justified as measured pH values can be subject to inaccuracy (see Fig. 1 supplementary material) due to the use of unpurified McP (Yao et al., 2007) whereas the accuracy of A_T and C_T measurements is controlled through the use of CRM. Thus, the estimated total error of the calculated $pCO_2{}^{SW}$ is 5.8 μatm (Millero, 1995). All the derived carbonate parameters are presented at *in situ* temperature.

2.4.3. Deconvolution of thermal and non-thermal processes on $pCO_2{}^{SW}$

Effects of non-thermal ($pCO_2{}^{N}$) and thermal ($pCO_2{}^{TD}$) processes on $pCO_2{}^{SW}$ variations have been calculated thereafter using following equations (2) and (3) (Takahashi et al., 1993, 2002):

$$pCO_2{}^{N} = pCO_2{}^{obs} \times e^{(0.0423(Tmean - Tobs))} \quad (2)$$

$$pCO_2{}^{TD} = pCO_2{}^{mean} \times e^{(0.0423(Tobs - Tmean))} \quad (3)$$

where pCO_2^{obs} is the pCO_2^{SW} calculated during the study period in surface (in µatm), pCO_2^{mean} is the mean pCO_2^{SW} over the study period in surface (402 µatm), T^{mean} is the average temperature (in °C, here T^{mean} = 16.90 °C) and T^{obs} is the *in situ* temperature (in °C).

pCO_2^{N} represents a temperature-normalised pCO_2^{SW}, and pCO_2^{TD} represents the changes pCO_2^{SW} induced by temperature fluctuations under isochemical conditions.

2.4.4. CO_2 fluxes between ocean and atmosphere

The air-sea CO_2 exchanges were calculated according to the equation described in Weiss (1974) and Wanninkhof (2014). The flux of CO_2, expressed in this paper in mmol $CO_2.m^{-2}.d^{-1}$, can be determined according to equation (4):

$$FCO_2 = k \times \alpha \times (pCO_2^{SW} - pCO_2^{ATM}) \quad (4)$$

where k is the gas transfer velocity for CO_2 (in $cm.h^{-1}$), α is the solubility coefficient of CO_2 (in $mol.L^{-1}.atm^{-1}$) calculated as a function of temperature and salinity (Weiss, 1974) and pCO_2^{SW} and pCO_2^{ATM} are the seawater and atmospheric partial pressure of CO_2, respectively (in µatm). By convention, a negative sign indicates a flux from the atmosphere to the ocean (Wanninkhof et al., 2013).

The relationship (5) of Wanninkhof (2014) is used to compute the gas transfer velocities:

$$k = 0.25l \times U_{10}^2 \times (Sc/660)^{-1/2} \quad (5)$$

where U_{10} is the wind speed (in $m.s^{-1}$) and Sc is the Schmidt number (dimensionless), calculated according to the equation in Wanninkhof (2014).

The air-sea CO_2 fluxes were estimated at the same time as the pCO_2^{SW} estimation. Because no atmospheric pCO_2 measurement is available at the SOLEMIO point, the mean pCO_2^{ATM} value (see section 2.3) for the week preceding the measurement of pCO_2^{SW} was used, this value being an estimate of the regional average pCO_2^{ATM} value for the sampling day. Due to the buffering effect, the weekly average wind speed estimate at the SOLEMIO was used in air-sea fluxes calculations.

2.4.5. Biological flux calculations

Net Ecosystem Calcification (NEC) of the system was calculated according to Eq. (6) (derived from Bensoussan and Gattuso (2007):

$$NEC = -0.5 \times \Delta A_T \times d \times \rho/\Delta t \quad (6)$$

where ΔA_T is the change in total alkalinity between sampling intervals (in $mmol.kg^{-1}$), d is the mixed layer depth (MLD) water (in meters), ρ is the *in situ* seawater density (in $kg.m^{-3}$) and Δt is the time interval between sample intervals (in days). NEC is in mmol $C.m^{-2}.d^{-1}$.

Net Ecosystem Production (NEP) was calculated according to Eq. (7) (derived from Borges et al., 2008) using changes in C_T from two consecutives sampling and correcting for additional changes associated with NEC and air-sea CO_2 gas exchanges (FCO_2) as:

$$NEP = -[\Delta C_T \times d \times \rho/\Delta t - NEC + FCO_2] \quad (7)$$

where ΔC_T is the change in C_T (in $mmol.kg^{-1}$) over the time period Δt (in days), d is the mixed layer depth (MLD) water (in meters), ρ is the *in situ* seawater density (in $kg.m^{-3}$), NEC is in mmol $C.m^{-2}.d^{-1}$ and FCO_2 is the average air-sea flux of CO_2 between two consecutive samplings (in mmol $CO_2.m^{-2}.d^{-1}$). NEP is in mmol $C.m^{-2}.d^{-1}$. To remove the impact of salinity variations (evaporation/precipitation) on A_T, salinity-normalised changes in A_T (and C_T) were calculated by dividing by *in situ* salinity and multiplying by 38. The remaining ΔA_T is assumed to be from calcification/dissolution. Nonetheless, because no significant relationship exists between C_T and the sea surface salinity at the SOLEMIO site, C_T has not been normalised to salinity for NEP calculations. Low Salinity Events (see section 4.2) have been removed from these calculations.

2.4.6. Statistic test

Linear relationships have been tested using the Pearson coefficient for parametric test (Sokal and Rohlf, 1969) with a significance level of 95%.

3. Results

3.1. Hydrography

The hydrographic conditions encountered at the SOLEMIO site are described in Fig. 2 with the time-series of temperature, salinity and MLD over the studied period (Fig. 2A, B and 2C) and the monthly mean values for temperature and salinity at the surface and bottom (Fig. 2D, E, 2F and 2G).

Over the two-years, the mean temperature was 16.90 °C at the surface and 14.65 °C at the bottom, with a maximum (23.42 °C) and minimum (12.94 °C) occurring both in surface waters in August 2017 and February 2018, respectively. Marked seasonal cycles were present for both depths (Fig. 2A, D and 2F) with an increase in temperature from May to October and a decrease from November to April. Based on the temperature data recorded at the SOLEMIO site from January 1997 to October 2019 (http://somlit.oasu.u-bordeaux.fr/mysomlit-public/), the hydrological situation for the period used in this manuscript shows that summers and winters were warmer than the reference situation in 1997, with an increase over the two-years. No extreme climatic event has been reported over the studied period.

Based on monthly means (Fig. 2E and G), the annual range in salinity at the SOLEMIO site was higher at the surface (from 36.82 to 38.36) than at the bottom (from 38.06 to 38.33). Over the two-year period, lower mean values of salinity are observed in the surface (38.07) than at the bottom (38.22) (Table 1). In this study, "Low Salinity Events" (LSE) will represent the sampling day where the recorded values of salinities were lower than 37.80 at the surface. LSE were recorded seven times at the SOLEMIO station over the studied period, mostly in spring and summer (Fig. 2B).

Based on MLD estimates, two hydrological "seasons" can be defined in the BoM: a well-mixed water column in winter ("winter" deep MLD between November and March included) and a summer thermal stratification period ("summer" shallow MLD between April and October included) with average MLD values of 41 ± 13 m in "winter" deep MLD conditions and of 20 ± 17 m in "summer" shallow MLD (Fig. 2C).

3.2. Nutrients

The variations in inorganic nutrient concentrations over the studied period are described in Fig. 2 of the supplementary material with a time-series for NO_3^-, NO_2^-, PO_4^{3-} and $Si(OH)_4$. NO_3^-, NO_2^- and PO_4^{3-} concentrations displayed smooth seasonal patterns, with a decrease during spring (March–April) reaching a minimum value, under the detection limit, in late spring or summer and an increase in autumn reaching a maximum value in winter (January–February). At the surface, concentrations ranged from non-detectable to 5.48 $µmol.L^{-1}$ for nitrate, from non-detectable to 0.64 $µmol.L^{-1}$ for nitrite and from non-detectable to 0.21 $µmol.L^{-1}$ for phosphate. Orthosilicic acid concentrations were never completely depleted in the water column. NO_3^-, NO_2^- and PO_4^{3-} concentrations were low at both depths throughout the studied period with lower concentrations at the surface than at the bottom (Table 1).

3.3. Carbonate system parameters

The variations in the carbonate system parameters are described in Fig. 3 with the time-series of C_T, A_T pH_T^{is} and pCO_2^{SW} over the studied period (Fig. 3A, B, 3C and 3D) and the monthly mean values at surface (Fig. 3E, F, 3G and 3H) and bottom (Fig. 3I, J, 3K and 3L).

At the surface, mean values of C_T were 2289 µmol kg^{-1} with maximum C_T values in winter (2359 µmol kg^{-1}, February 2018) and minimum values in the late summer (2248 µmol kg^{-1}, October 2016). The mean C_T concentration observed at the bottom (C_T = 2303 µmol kg^{-1})

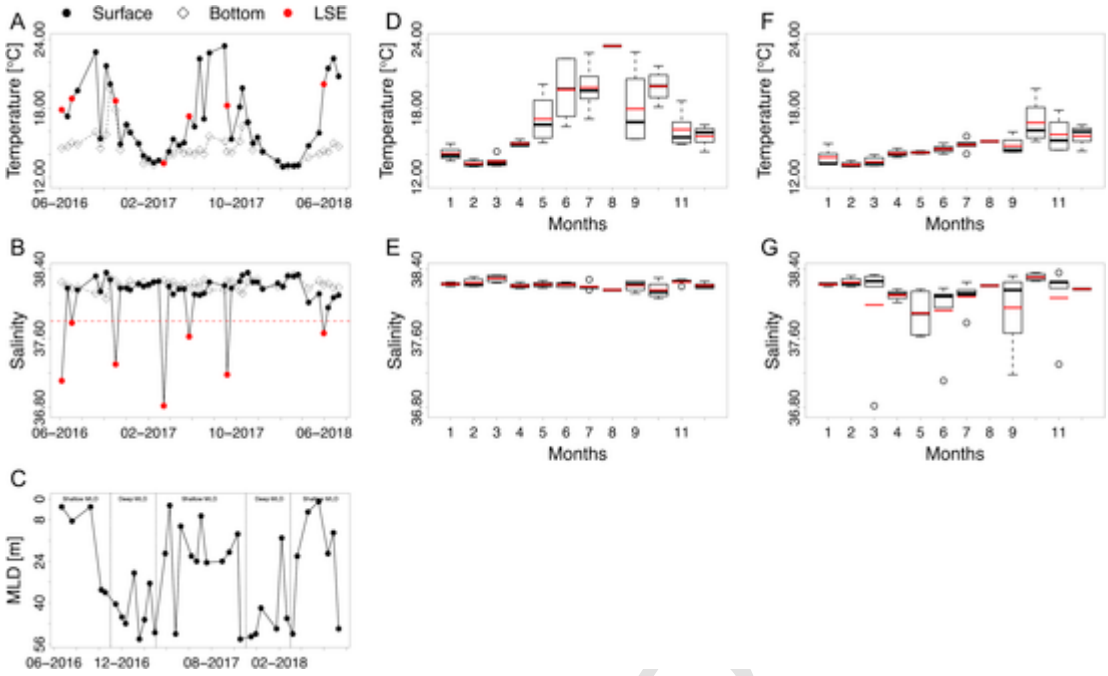

Fig. 2. Time-series observations for temperature (A), salinity (B) and Mixed Layer Depth (MLD – C) and box plots of pooled monthly temperature and salinity at the SOLEMIO site at 1 m (black circles and solid line; Fig. 2D and E) and at the bottom (55 m – white diamonds and dotted line; Fig. 2F and G) from June 2016 to July 2018. In figures (A) and (B), red points represent Low Salinity Events (LSE), and the red dotted line represents a salinity equal to 37.8. In box plots are shown the median (black line), the mean (red line), the first (Q1), and third quartiles (Q3) and data outliers (dotted lines). (For interpretation of the references to colour in this figure legend, the reader is referred to the Web version of this article.)

Table 1
Time-series analyses on seawater carbonate chemistry at the SOLEMIO site for temperature (Temp.), salinity, pH_T measured *in situ* (pH_{Tis}), total alkalinity (A_T), dissolved inorganic carbon (C_T), partial pressure of CO2 (pCO_2), nitrate (NO_3^-), nitrite (NO_2^-), phosphate (PO_4^{3-}), orthosilicic acid ($SiOH_4$), calcite (Ω_C) and aragonite (Ω_A) saturation states, from June 2016 to July 2018, at 1 m and at the bottom (55 m). SD stands for standard deviation. DL stands for Detection Limit.

SURFACE	Mean ± SD	Min. – Max.	BOTTOM	Mean ± SD	Min. – Max.
Temp. [°C]	16.90 ± 3.16	12.94–23.42	Temp. [°C]	14.65 ± 1.33	12.93–19.71
Salinity	38.07 ± 0.34	36.82–38.36	Salinity	38.22 ± 0.06	38.06–38.33
pH_{Tis}	8.086 ± 0.028	8.015–8.121	pH_{Tis}	8.091 ± 0.018	8.053–8.129
A_T [µmol.kg-1]	2584 ± 18	2554–2624	A_T [µmol.kg-1]	2582 ± 15	2560–2621
C_T [µmol.kg-1]	2289 ± 27	2248–2359	C_T [µmol.kg-1]	2303 ± 20	2256–2358
pCO_2 [µatm]	402 ± 31	358–471	pCO_2 [µatm]	394 ± 21	362–439
NO_3^- [µmol.L^{-1}]	0.78 ± 1.07	<DL – 5.48	NO_3^- [µmol.L^{-1}]	1.16 ± 0.94	0.03–3.5
NO_2^- [µmol.L^{-1}]	0.09 ± 0.12	<DL – 0.64	NO_2^- [µmol.L^{-1}]	0.14 ± 0.11	0.01–0.42
PO_4^{3-} [µmol.L^{-1}]	0.05 ± 0.04	<DL – 0.21	PO_4^{3-} [µmol.L^{-1}]	0.05 ± 0.04	<DL – 0.14
$SiOH_4$ [µmol.L^{-1}]	1.63 ± 0.65	0.41–4.50	$SiOH_4$ [µmol.L^{-1}]	1.86 ± 0.59	0.43–3.46
Ω_C	4.99 ± 0.33	4.44–5.64	Ω_C	4.67 ± 0.23	4.23–5.29
Ω_A	3.23 ± 0.24	2.85–3.70	Ω_A	3.01 ± 0.16	2.72–3.45

was higher than at the surface with no clear seasonal trend. Higher monthly variability of C_T is observed during autumn and winter than during spring and summer (Fig. 3E and I).

Mean value of A_T was similar at the bottom (A_T = 2582 µmol kg^{-1}) to that at the surface (A_T = 2584 µmol kg^{-1}). A_T ranged from 2554 µmol kg^{-1} (June 2018) to 2624 µmol kg^{-1} (November 2017) and did not show, at either depth, clear seasonal trends (Fig. 3B, F and 3J). A_T presents a broad variability (Fig. 3F and J) within summer and autumn months.

A surface pH_T^{is} average value of 8.086 is observed with the lowest value in summer (8.015, July 2017) and highest value in late winter (8.121, March 2017). Surface pH_T^{is} values present a higher variability in summer than in winter (Fig. 3G).

pCO_2^{SW} ranged from 471 µatm (July 2017) to 358 µatm (November 2017) with a surface mean value of 402 µatm (Table 1, Fig. 3D). Large monthly variability of pCO_2^{SW} is observed in summer at the surface (Fig. 3H). The highest pCO_2^{SW} values were observed in the summer months of 2017 and 2018 compared to the increase observed in 2016. Monthly means distributions of pCO_2^{SW} in the surface displayed a clear seasonal trend with values starting to increase in late spring, reaching maximum values in summer and then a decreasing trend from September onward.

Calcite and aragonite saturation states reveal that BoM waters were oversaturated ($\Omega > 1$) with both minerals throughout the entire water column (Table 1). Mean saturation state for calcite was 4.99 at the surface, and 4.67 at the bottom. For aragonite, the mean saturation state was 3.23 at the surface, 3.01 at the bottom. These saturation state estimates are considered as a general description of the carbonate system in the bay but will no longer be discussed in this study.

3.4. Air-sea CO_2 fluxes

As no pCO_2^{ATM} was directly recorded over the BoM, two pCO_2^{ATM} "end member" datasets are considered in order to estimate a realistic range of air-sea fluxes: the urbanised 5Av site (Fig. 1), representing the higher mean pCO_2^{ATM} value in the city of Marseille with the weekly

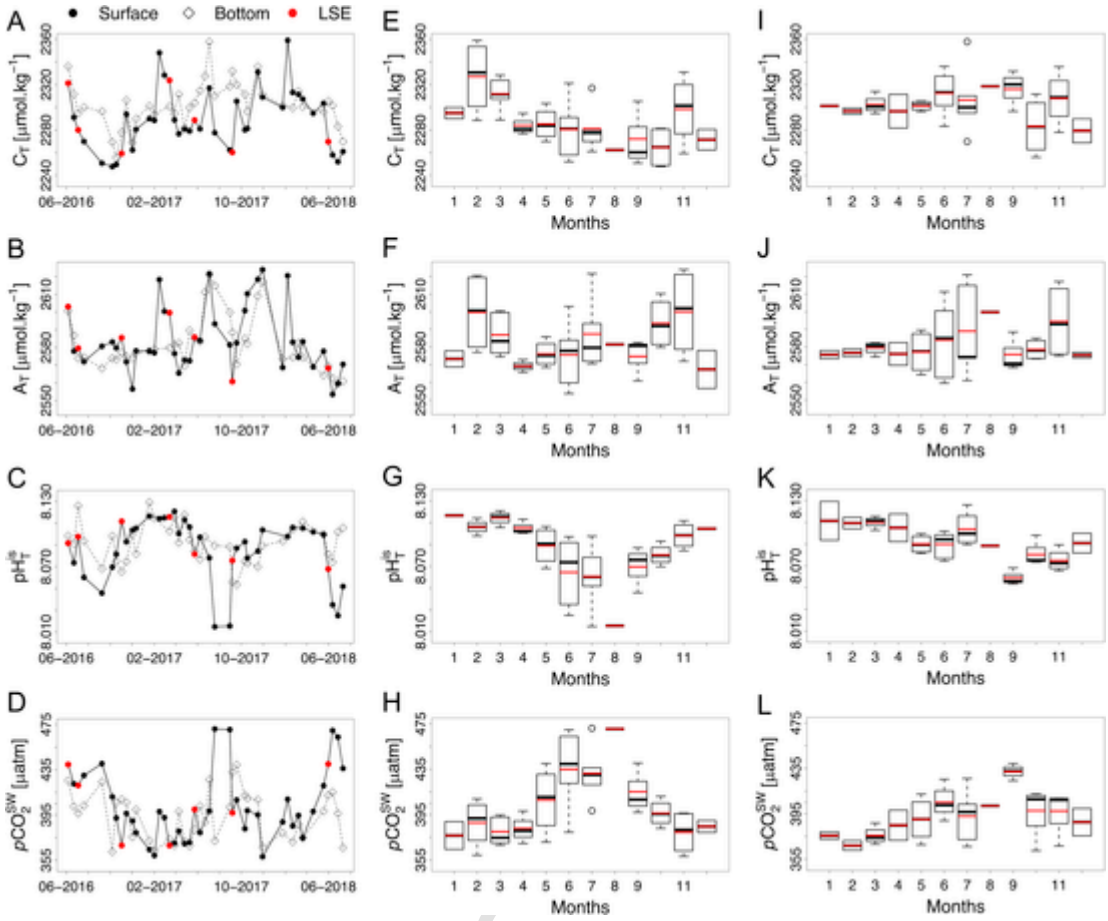

Fig. 3. Time-series observations for seawater carbonate parameters (A, B, C, D) and box plots of pooled monthly seawater carbonate parameters at the SOLEMIO site at 1 m (black circles and solid line; Fig. 3E, F, 3G, 3H) and at the bottom (55 m – white diamonds and dotted line; Fig. 3I, J, 3K, 3L) from June 2016 to July 2018. In figures (A, B, C, D), red points represent Low Salinity Events (LSE). In box plots are shown the median (black line), the mean (red line), the first (Q1), and third quartiles (Q3) and data outliers (dotted lines). (For interpretation of the references to colour in this figure legend, the reader is referred to the Web version of this article.)

mean values ranging between 399.9 and 454.3 µatm, and the OHP site (Fig. 1), representing the regional background pCO_2^{ATM} with values ranging between 390.4 and 416.5 µatm.

The estimated mean daily air-sea CO_2 values are −0.7 mmol $C.m^{-2}.d^{-1}$ (corresponding to −255 mmol C $m^{-2}.a^{-1}$) and −2.2 mmol $C.m^{-2}.d^{-1}$ (corresponding to −803 mmol C $m^{-2}.a^{-1}$), with pCO_2^{ATM} recorded at the OHP site and the 5 Av site, respectively. Fig. 4 shows positive flux values in summer and spring for both atmospheric pCO_2 datasets used, and negative values in winter and autumn.

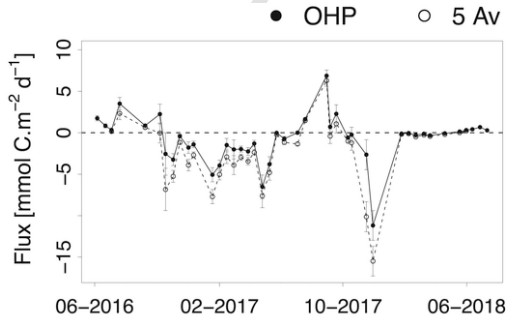

Fig. 4. Time-series observations of the air-sea CO_2 flux (Flux in mmol $C.m^{-2}.d^{-1}$) with atmospheric pCO_2 measured at the OHP site (full circle) and at the 5 Av site (empty circle) and with pCO_2^{SW} measured at the SOLEMIO site from June 2016 to July 2018. Error bars indicate errors of the associated variables of the formula used. By convention, a negative flux indicates fluxes directed from the atmosphere to the ocean, and a positive flux indicates fluxes directed from the ocean to the atmosphere.

4. Discussion

4.1. Comparison with existing carbonate data in the Mediterranean

In the Ligurian Sea, a time-series of carbonate chemistry from the observation network MOOSE exists at the DYFAMED and ANTARES sites. Moreover, in the Bay of Villefranche-sur-Mer (Point B), a time-series of carbonate chemistry is recorded within the framework of the SOMLIT observational network (Fig. 1).

When compared to Point B station data (Table 2), mean values for A_T and C_T in the BoM are higher by *ca.* 30 µmol kg^{-1} and 50 µmol kg^{-1}, respectively. Even when normalised to salinity, this discrepancy remains. The seasonal trend observed for C_T is comparable to the seasonal trend at Point B, whereas the seasonal variation for A_T in the surface waters at this site was not observed in the BoM. The higher variability observed mostly during the summer in the BoM has also been observed by Kapsenberg et al. (2017) at the Point B site and is related to temperature variability.

For the two Ligurian open ocean time-series, the same differences with the BoM are observed. A_T and C_T values were lower by *ca.* 20 µmol kg^{-1} and 30 µmol kg^{-1} for ANTARES, and by *ca.* 15 µmol kg^{-1} and 20 µmol kg^{-1} for DYFAMED. Here again, when normalised to salinity, higher A_T and C_T are still observed in the BoM. The Rhone River waters have higher A_T concentrations which could impact the A_T values of the BoM. The LSE could be associated to the inflow of Rhone River water in the BoM (see section 4.2). However, when excluding LSE values from the BoM dataset, the observed differences with the three other Mediterranean time-series remains (see Table 2 in supplementary material). It has to be mentioned that the BoM time-series corresponds to a

Table 2
A_T and C_T mean values in the Ligurian Sea (Point B, DYFAMED and ANTARES) and in the Bay of Marseille (SOLEMIO). Salinity-normalised changes in A_T (nA_T) and C_T (nC_T) were calculated by dividing by *in situ* salinity and multiplying by 38. SD stands for standard deviation.

	Depth	SOMLIT (2016–2018)	Point B (2007–2016)	DYFAMED (1998–2016)	ANTARES (2010–2017)
A_T [µmol.kg $^{-1}$]	Surface	2584 ± 18	2555 ± 13	2568 ± 13 (0–50 m)	2563 ± 22 (0–50 m)
	Bottom	2582 ± 15	2553 ± 12		
C_T [µmol.kg $^{-1}$]	Surface	2289 ± 27	2242 ± 19	2272 ± 30 (0–50 m)	2262 ± 34 (0–50 m)
	Bottom	2303 ± 20	2249 ± 17		
nA_T [µmol.kg $^{-1}$]	Surface	2580 ± 30	2559 ± 17	2548 ± 8 (0–50 m)	2550 ± 18 (0–50 m)
	Bottom	2567 ± 16	2551 ± 9		
nC_T [µmol.kg $^{-1}$]	Surface	2286 ± 35	2246 ± 26	2254 ± 27 (0–50 m)	2251 ± 30 (0–50 m)
	Bottom	2289 ± 19	2248 ± 17		
Reference	/	/	Kapsenberg et al. (2017)	Coppola et al. (2018)	Lefèvre (2010)

more recent period than the other time-series. However, if an open ocean increase of 1 µmol $kg^{-1}.a^{-1}$ in C_T in response to the atmospheric increase in CO_2 is assumed (Merlivat et al., 2018), the differences in C_T cannot be explained due to time lag in sampling. In this coastal area, it is worth noting that terrestrial discharges coming from the Rhone River and wastewater treatments can lead to an increase of A_T as allochthonous matter (see Fig. 2 in supplementary material) can be associated with non-carbonate alkalinity (Hunt et al., 2011; Soetaert et al., 2007). Moreover, because A_T and C_T measurements were performed simultaneously in a closed cell, the increase on A_T could lead to repercussion on C_T determination (Dickson, 2007). Both consequences of the presence of allochthonous material could affect the derived carbonate parameters. This effect, certainly marginal, cannot be quantified with the present dataset.

The seasonal and monthly variability of the pH_T^{is} observed in the BoM shows a similar dynamic to that of the Bay of Villefranche (Kapsenberg et al., 2017). For both sites this dynamic is mostly driven by the temperature variations. For pCO_2^{SW}, a seasonal trend with higher values during the summer period and lower values during the winter period occurs in the BoM highlighting the close relationship between pCO_2^{SW} and seawater temperature. This pattern has already been reported for the coastal point B site (Kapsenberg et al., 2017) but also the open ocean DYFAMED site, where temperature changes can induce strong seasonal variation in pCO_2^{SW} values, varying between 300 and 500 µatm (Copin-Montégut et al., 2004; Hood and Merlivat, 2001; Merlivat et al., 2018).

For the air-sea CO_2 fluxes, there are a few studies indicating that the NW MedSea is a CO_2 sink. In the Villefranche Bay, De Carlo et al. (2013) measured average annual fluxes (using the Ho et al. (2006) formula for gas transfer velocity) of −191 mmol C $m^{-2}.a^{-1}$. In the Ligurian Sea, at the DYFAMED site, the average annual flux (using the Wanninkhof and McGillis (1999) formula for gas transfer velocity) was estimated to be −319 mmol C $m^{-2}.a^{-1}$ from February 1998 to January 1999, and -682 mmol C $m^{-2}.a^{-1}$ from February 1999 to January 2000 (Copin-Montégut et al., 2004). In the Gulf of Trieste, Ingrosso et al. (2016) reported mean annual fluxes of −781 ± 931 mmol $C.m^{-2}.a^{-1}$ and of −1194 ± 2117 mmol $C.m^{-2}.a^{-1}$ in 2012 and 2013, respectively. The average flux calculated at the SOLEMIO station, with pCO_2^{ATM} recorded at the OHP site, lies between the annual fluxes recorded at these three sites. With pCO_2^{ATM} recorded at the 5 Av site, air-sea CO_2 fluxes are higher than those previously obtained in the Ligurian Sea and closer to those estimated in the Adriatic Sea. It is worth mentioning that for both studies used in this comparison (DYFAMED and Villefranche Bay), pCO_2^{ATM} values from Lampedusa Island are used and that at high wind speeds (>10 m s^{-1}) (Table 3), large differences between gas transfer velocity formulations appear (Ho et al., 2006).

4.2. Influence of low salinity events on A_T/salinity relationships

A_T is considered as a conservative quantity with respect to water mixing (Wolf-Gladrow et al., 2007). When biological activity is excluded, the variations of A_T should be directly related to salinity changes when dilution or evaporation occurs in the ocean. In consequence, A_T concentrations are generally related to salinity through a linear relationship (Copin-Montégut, 1993). Indeed, for sub-tropical oceans, the salinity contribution to the surface A_T variability has been estimated to be greater than 80% (Millero et al., 1998). In the MedSea, several linear relationships between A_T and salinity in the surface waters have been proposed for different sub-basins (*e.g.*, Copin-

Table 3
Distributions of salinity measured at the SOLEMIO site, the Rhone River discharge water ($m^3.h^{-1}$), the precipitation rate (mm), the wind direction (°) and speed ($m.s^{-1}$) and maximum and minimum salinity values measured by the four buoys of the STPS network (see Fig. 1) for the seven observed LSE.

	June 6th, 2016	July 4th, 2016	November 2nd, 2016	March 15th, 2017	May 24th, 2017	September 6th, 2017	May 31st, 2018
Salinity measured	37.11	37.78	37.30	36.82	37.62	37.18	37.66
RR flow [$m^3.h^{-1}$]	2650	1400	850	2020	1200	630	2300
Precipitation [mm]	$2.16.10^{-3}$	$2.89.10^{-8}$	$1.39.10^{-2}$	$6.27.10^{1}$	$1.50.10^{2}$	$7.57.10^{-4}$	NA
Wind direction [°]	174	282	NA	203	322	NA	289
Wind speed [$m.s^{-1}$]	3.46	1.84	5.66	1.99	1.84	11.19	2.44
STPS Balancelle buoy (Smin – Smax)	12.49–32.36	21.86–37.63	22.33–37.08	11.83–35.04	16.98–34.61	35.19–37.19	14.72–36.99
STPS Omega buoy (Smin – Smax)	19.54–30.29	31.42–34.20	NA – NA	25.79–35.38	33.65–37.30	34.08–37.35	NA – NA
STPS Carro buoy (Smin – Smax)	24.90–36.84	30.77–37.51	35.87–37.99	23.08–36.65	28.82–35.29	30.97–36.15	37.37–37.86
STPS Carry buoy (Smin – Smax)	29.38–37.49	31.72–34.28	33.36–38.29	32.79–37.93	35.45–37.79	33.16–35.97	37.24–37.70

Montégut and Bégovic, 2002; Hassoun et al., 2015; Ingrosso et al., 2016; Rivaro et al., 2010; Schneider et al., 2007). However, in the BoM, over the two-year time-series considered, no significant linear relationship between surface A_T and surface salinity has been observed (Fig. 5) (r = 0.048, n = 45, p-value = 0.762).

Based on A_T values collected over a large part of the MedSea, Schneider et al. (2007) have demonstrated that freshwater inputs from rivers affect the A_T-S relationship in the MedSea due to high A_T values of riverine inputs. This is the case for the Rhone River waters which give high alkalinity values of *ca.* 2885 μmol kg^{-1} (GEMSWATER data in Schneider et al., 2007).

The hourly surface salinity data collected from the STPS buoy network (extracted four days before, and two days after the sampling day at SOLEMIO - see methods) indicates that the seven observed LSE reported in section 3.1 are associated to the occurrence of a Rhone River plume Eastward along the coast. Moreover, the offshore wind conditions (NW/N) during the prevailing period (Table 3) confirms a possible eastward extension of the Rhone plume before and during LSE observed in BoM, as demonstrated by Gangloff et al. (2017). Also, low rainfall rates have been recorded the preceding week of the LSE. This observation sustains the scenario that these LSE are due to intrusions of freshwater coming from the Rhone River in the surface of the BoM.

When these intrusions of Rhone River water occur, the sea surface salinity is lowered (down to 36.82), but due to the elevated alkalinity values of the Rhone River, they do not induce a decrease in the A_T values (Fig. 5). In consequence, the intrusion of Rhone River water during LSE can explain the deviation from the A_T-S linear relationship. Indeed, when the seven LSE values are not considered, a significant linear relationship is observed between A_T and S (r = 0.413, n = 38, p-value = 0.014).

4.3. Driving forces of the air-sea CO_2 exchanges in the BoM

Over an annual cycle the BoM acts alternatively as a source or a sink of CO_2 due to seasonal variability in the air-sea fluxes (mostly driven by the pCO_2^{SW}). Nevertheless, as observed in other parts of the NW MedSea, on an annual scale, the BoM is a potential atmospheric CO_2 sink.

In addition to the gas solubility, air-sea CO_2 fluxes are controlled by the piston velocity and the pCO_2 difference between seawater and atmosphere (see equation (4)). The contribution of these different terms to air-sea CO_2 flux variability in the BoM can be deciphered from the variability of these different contributions.

Changes of CO_2 partial pressure in the ocean (pCO_2^{SW}) are due to combined effects of biological and physical processes. Following the approach proposed by Takahashi et al. (1993, 2002), the respective contributions of thermal and non-thermal processes on pCO_2^{SW} have been estimated (see section 2.4.3). Fig. 6A reveals consistent seasonal trends between pCO_2^{SW} and pCO_2 induced by temperature changes (pCO_2^{TD}). Contributions of thermal (pCO_2^{TD}) and non-thermal processes (pCO_2^{N}) on pCO_2^{SW} are presented in Fig. 6B. The main variation of pCO_2^{SW} occurs because of changes in surface seawater temperature, with a contribution of the thermal parameter (pCO_2^{TD}) to the changes in pCO_2^{SW} varying from +113 μatm (generated by warming) to −75 μatm (due to cooling) (Fig. 6B), for an overall range of 188 μatm.

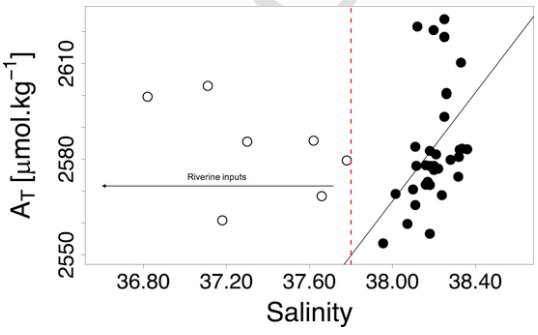

Fig. 5. A_T vs. Salinity relationship at the SOLEMIO site (1 m). Red dotted line corresponds to a salinity value equal to 37.8. Empty circles represent A_T values measured at salinity under 37.8 (Low Salinity Events) and objectively excluded from the regression. (For interpretation of the references to colour in this figure legend, the reader is referred to the Web version of this article.)

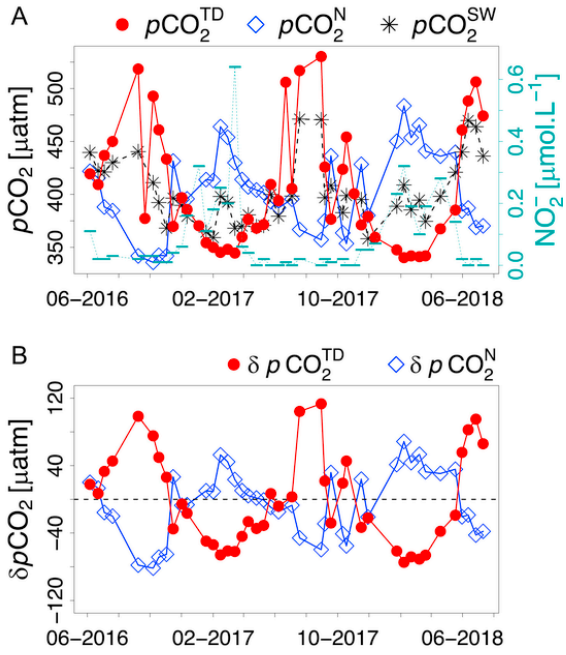

Fig. 6. (A) Time-series observation for surface seawater pCO_2^{TD} (pCO_2 changes induced by temperature (Temp-Driven); red line), surface seawater pCO_2^{N} (pCO_2 changes induced by to non-thermal effect; blue line), surface seawater pCO_2 (pCO_2^{SW}; black line) and nitrite (NO_2^-) concentrations (green line) at the SOLEMIO site from June 2016 to July 2018. (B) Changes in pCO_2 that can be attributed to changes in temperature, calculated as: $\delta pCO_2^{TD} = pCO_2 - pCO_2^{N}$, and changes in pCO_2 that can be attributed to non-thermal effects, calculated as: $\delta pCO_2^{N} = pCO_2 - pCO_2^{TD}$. The pCO_2^{N} and pCO_2^{TD} used in the above equations correspond to Eqs. (2) and (3) in the text, respectively. (For interpretation of the references to colour in this figure legend, the reader is referred to the Web version of this article.)

Variations in pCO_2^{SW} induced by non-thermal processes (pCO_2^{N}) showed a regular pattern, with a seasonal maximum in winter to a minimum in summer (Figs. 6A and 4). The pCO_2^{N} variability is mainly due to biological activity, but it also includes changes due to advection, vertical diffusion and air-sea gas exchanges (De Carlo et al., 2013). The pCO_2^{N} varies at the surface from +69 μatm in winter to −82 μatm in late summer (Fig. 6B). In the BoM, freshwater intrusions have a crucial influence on efflorescence events which are punctual and brief (Diaz et al., 2008; Fraysse et al., 2014). The biological component being poorly represented by bi-monthly sampling of Chl-A (Fig. 2 in supplementary material), pCO_2^{N} could not be completely related to this parameter. Variations of pCO_2^{N} are partially synchronous with those of C_T (Figs. 3A and 6A), mostly in winter. There is a more pronounced synchronous link between nutrients (and in particular the nitrite concentrations) and pCO_2^{N}. The high concentrations of nitrite in winter could be an indirect evidence of increased organic matter remineralisation by heterotrophic activity. Indeed, the activity of heterotroph remineralisation releases high contents of ammonium into the seawater (Kirchman, 2000). This accumulated ammonium might then have been oxidised into nitrite through bacterial nitrification which is, furthermore, favoured in the low light conditions found in winter (Ward, 1985). Thus, the observed nitrite accumulation would result from nitrifying oxidation of ammonium (Meeder et al., 2012; Zakem et al., 2018) and could indirectly sign a strengthened remineralisation of organic matter, especially in winter. The oxidation of organic matter by aerobic respiration producing well higher contents of CO_2 than that consumed by nitrifying bacteria (Zakem et al., 2018), it is then possible to observe increased quantities of NO_2^- concomitantly to increased concentrations of C_T and pCO_2^{N}.

The increase in nitrite concentrations observed during winter, concomitant with the pCO_2^N increase, might indicate that heterotrophic processes significantly contribute to the CO_2 content of seawater at certain periods of the year (*i.e.* winter).

These calculated pCO_2^N and pCO_2^{TD} highlight the concomitant impacts of biological activity and physical processes on the pCO_2^{SW} variations. During spring, depending on the nutrient availability, the increase in pCO_2 by seawater warming is counteracted by the photosynthetic uptake that simultaneously lowers C_T and nutrients stocks. Then, as the nutrient availability becomes less, biological CO_2 consumption decreases in autumn and heterotrophic respiration leads to an increase in the C_T and pCO_2^N values. Moreover, during winter, seawater cooling tends to decrease pCO_2 and this process could also be counteracted by the mixing of bottom-water enriched in C_T with the deepening of the MLD (Fig. 2C). The temperature in the upper layer of the MedSea is increasing (Nykjaer, 2009; Vargas-Yáñez et al., 2008). Since 1997, the temperature at the SOLEMIO site has increased (see section 3.1). Because of the temperature predominance on the control of the pCO_2^{SW} signal, this warming tendency should induce higher pCO_2^{SW} values in the surface layer. This could induce an increased stratification of the water column, which could decrease the available nutrients in the euphotic zone. Therefore, less pCO_2 could be counterbalanced by non-thermal processes, making the effect of increasing pCO_2^{SW} even stronger.

Changes of CO_2 partial pressure in the atmosphere (pCO_2^{ATM}) in the BoM are characterised by the regional background concentration on top of which is added the effect of the urbanised Marseille area. In order to highlight the anthropogenic impact of the Marseille Metropolis on the BoM, two pCO_2^{ATM} datasets have been used (see section 3.4). The CO_2 sink increases with increasing pCO_2^{ATM} values, as seen when using pCO_2^{ATM} values from the 5 Av station (Fig. 4, dotted line). It is worth noting that in this urbanised area, the pCO_2^{ATM} daily variation is almost 38 μatm on average with some events exceeding 150 μatm. Thus, this study shows that high pCO_2^{ATM}, as observed in coastal anthropised areas, may increase the sink of CO_2 in the surrounding marine waters.

Finally, the effect of the piston velocity on the CO_2 exchanges is highly dependent on the wind speed. Indeed, at wind speeds above 7–10 m s^{-1}, the piston velocity increases considerably. At the SOLEMIO site, wind speeds ranging between 5 and 13 m s^{-1} were detected during *ca.* 45% of the time. In the BoM, the highest CO_2 in-gasing value (November 2017) is associated with the strongest daily wind episode (12 m s^{-1}) and low pCO_2^{SW} (358 μatm). This illustrates the potential importance of short scale events on the piston velocity of the air-sea exchanges variability (Ingrosso et al., 2016). At a windy site like SOLEMIO, the high pCO_2^{ATM} and high wind periods could have a noticeable impact on the air-sea CO_2 fluxes. For example, Copin-Montégut et al. (2004) reported significant differences in the air-sea CO_2 fluxes in 1998 and 1999 because of strong winds during the autumn of 1999. However, Xueref-Remy et al. (2018) highlighted the fact that the amplitude of the atmospheric CO_2 concentration range, and especially the maximum values, decrease exponentially with wind speed because of the ventilation and dilution effects in the atmosphere.

In general, at the SOLEMIO site, the time-series of the air-sea fluxes (Fig. 4) displays seasonal changes, for both OHP and 5 Av series, with CO_2 outgasing in summer, and ingasing in winter. This observation indicates that temperature, rather than biological processes, mostly drives the difference in pCO_2 between the ocean and the atmosphere and is certainly the main contributor to the air-sea CO_2 exchange variability. Nonetheless, episodic wind events, through the increase in the piston velocity, can significantly impact the air-sea CO_2 fluxes over shorter time scales (daily to weekly).

4.4. Is the biological contribution to the air-sea CO_2 fluxes significant?

In a given water mass, biological processes can modify the carbonate chemistry variables and thus affect the air-sea CO_2 exchanges. In the conceptual working frame proposed by Borges et al. (2006), the relationship between air-sea CO_2 fluxes and net ecosystem production (NEP) should be linear. In coastal environments, the physical forcing (such as coastal upwelling) and net ecosystem calcification (NEC) can also modulate the carbonate chemistry properties and therefore these subsequent fluxes, making the link between air-sea CO_2 fluxes and the ecosystem metabolism increasingly complex.

In the BoM, no direct measurements of ecosystem productivity were available during the period of this study. Oxygen derived estimations for ecosystem production based on Apparent Oxygen Utilisation are not relevant in the MLD due to the short equilibration time of pO_2 at the air-sea interface. Based on the approach proposed in Oudot (1989), a mean equilibration time of pO_2 of 2 days is estimated for this study. To accurately estimate *in situ* metabolic rates based on carbonate chemistry variations, high temporal resolution sampling over full dial cycles (24 h) is required. Moreover, to derive such estimates, it is assumed that the studied system is a closed system, or the residence times should be considered with respect to the high NEC estimates sensitivity to this parameter (Courtney and Andersson, 2019). No direct information on water mass residence time were available for the present study. Nevertheless, estimations of NEC and NEP are based on a simple assumption: the fortnightly temporal variations of A_T and C_T are driven by biological processes.

Because the MLD constitutes one of the major factors controlling ocean primary production (Sverdrup, 1953), mean values for NEC, NEP and air-sea CO_2 fluxes are reported for the two defined MLD seasons in Table 1 in the supplementary material. At the SOLEMIO site, the NEC daily mean value (2.9 ± 22.5 mmol $C.m^{-2}.d^{-1}$) suggests a net calcifying system, which is in accordance with the estimated calcite and aragonite saturation states. Also, estimated NEP mean values of 5.0 ± 116.8 mmol $C.m^{-2}.d^{-1}$ and 9.0 ± 29.2 mmol $C.m^{-2}.d^{-1}$ in winter and summer (with atmospheric pCO_2 reference from the OHP site), respectively, suggest that the BoM is a system where autotrophic processes prevail over heterotrophic processes. Over the studied period, the daily NEP presents a mean value equal to 7.3 ± 77.1 mmol $C.m^{-2}.d^{-1}$.

The CO_2 fluxes and trophic status of the BoM are presented in Fig. 7 within the conceptual frame proposed by Borges et al. (2006).

The mean air-sea CO_2 fluxes and NEP values are in good agreement with this conceptual frame with an ecosystem where autotrophic processes are associated to a sink of CO_2. Nonetheless, some of the results are in contradiction to this conceptual frame: in the BoM, negative NEP values (heterotrophic status) are associated with an atmospheric CO_2 sink (particularly in winter).

In order to explain this apparent contradiction, beside the errors associated to the NEP (and NEC) estimations, several reasons can be put forward: (1) In the Bay of Palma (NW MedSea), Gazeau et al. (2004) reported a similar observation which was related, at least partially, to the short residence time of the water mass in the bay (*ca.* 5 days). Water masses are then almost immediately flushed, and biological processes have a small impact on air-sea CO_2 fluxes. In the BoM, Millet

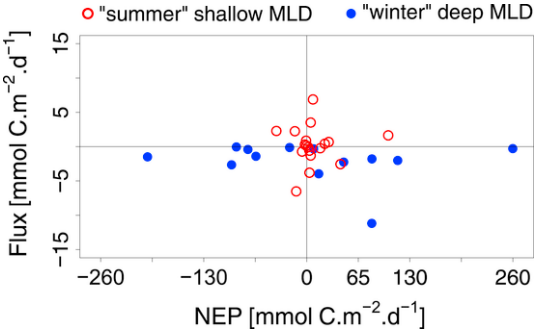

Fig. 7. Air-sea CO_2 fluxes (mmol $C.m^{-2}.d^{-1}$) from the OHP site versus Net Ecosystem Production according to the Mixed Layer Depth at the SOLEMIO site from June 2016 to July 2018. By convention, positive and negative NEP suggests an autotrophic status and a heterotrophic status, respectively. A negative FCO_2 sign indicates a flux directed from the atmosphere to the ocean while a positive FCO_2 sign indicates a flux directed from the ocean to the atmosphere. Data are divided into "winter" deep MLD (November to March; blue dot) and "summer" shallow MLD (April to October; red dot) in order to compare seasonal changes. (For interpretation of the references to colour in this figure legend, the reader is referred to the Web version of this article.)

et al. (2018) have measured a 5–10 day time-lapse for some particles to reach different locations around the BoM after their release, which indicates a short residence time of the water. This could partially explain the observed discrepancy with the conceptual frame. (2) In addition to NEP biological contribution, calcification/dissolution can affect the air-sea CO_2 fluxes. In the BoM, Bensoussan and Gattuso (2007) measured a NEC mean value of 8 mmol $C.m^{-2}.d^{-1}$. Despite this estimation being an order of magnitude lower in winter in this study, the importance of benthic communities in this shallow system could contribute, to some extent, to the air-sea CO_2 fluxes. (3) Also, there is an order of magnitude between the air-sea CO_2 exchanges and the metabolic flux intensity (Fig. 7), undermining the biological signature on the *in situ* carbonate chemistry. (4) Finally, temperature changes will further modulate the exchange of CO_2 through its impact on pCO_2^{SW}. In the BoM, most of the pCO_2 changes are related to the thermal effects (see section 4.3) and are probably the main reason for the apparent contradiction between the NEP and the air-sea CO_2 exchange. Thus, the sink of atmospheric CO_2 over the BoM seems to be impacted by the physical processes with a marginal contribution of biological processes. Nonetheless, considering the clear sampling limitations on NEP and NEC estimations, this work underlines the need for appropriate temporal and spatial resolution in a dedicated biological study.

5. Conclusions

Based on a two-year time-series, this paper presents the variability of the seawater carbonate system parameters in a Mediterranean coastal site close to the second largest city in France, Marseille. Based on sampling on a low temporal and spatial resolution, the air-sea CO_2 flux estimations in the BoM are, on average, directed from the atmosphere to the ocean. Temperature is the main force driving pCO_2^{SW} variability and it also has a major control on the air-sea CO_2 fluxes. As a result, temperature is the main driving force of the carbonate system variability in the bay. In the case of a windy site like SOLEMIO, the high $pCO_2^{A\text{T}\text{M}}$ and high wind periods have a significant impact on the air-sea CO_2 fluxes during episodic events through the wind effect on the gas transfer velocity. Episodic hydrodynamic events, such as the LSE processes, can also modify the biogeochemical composition of the BoM. However, this study shows the singularity of marine environments located at the border of highly urbanised areas characterised by high amplitudes of $pCO_2^{A\text{T}\text{M}}$ due to anthropogenic activity.

In a coastal zone like the BoM, in addition to the hydrodynamic structure of the area, this manuscript highlights the need to sample concomitantly *in situ* atmospheric and oceanic reservoirs. Various physical forcing affects the bay (*i.e.* Rhone River water intrusion, atmospheric forcing with highly variable CO_2 concentration) on a daily and hourly scale and this could not be resolved here. This study highlights the crucial need to develop integrated observation systems in order to measure the variability in carbon content at a high frequency in all reservoirs (ocean, atmosphere, biosphere). With an adapted temporal resolution of the physical forcing, the biological CO_2 fluxes in this coastal ecosystem should also be estimated in order to better understand the link between the metabolic status and the air-sea CO_2 exchanges. Finally, to focus on the ecosystem functioning, dedicated studies should be carried out to monitor key species dynamics, with an emphasis on calcifying species (pelagic and benthic), to follow the potential effect of oceanic acidification on the biodiversity.

Data availability: Time series data from the SOLEMIO site can be found at http://somlit.oasu.u-bordeaux.fr/mysomlit-public and are available at http://somlit.epoc.u-bordeaux1.fr/fr/. Carbonate system data presented in this paper are available on request from the corresponding authors. Atmospheric CO_2 data can be found online at https://icos-atc.lsce.ipsl.fr/OHP and www.atmosud.org/donnees/acces-par-station/. Requests for atmospheric CO_2 data should be addressed to irene.remy-xueref@univ-amu.fr and alexandre.armengaud@airpaca.org.

Fundings

This study takes part of the AMC project (Aix-Marseille Carbon Pilot program through the A*MIDEX project ANR-11-IDEX-0001-02), funded by the French National Research Agency (ANR). The project leading to this publication has received funding from European FEDER Fund under project 1166-39417.

CRediT authorship contribution statement

Cathy Wimart-Rousseau: Writing - original draft, Writing - review & editing, Visualization, Conceptualization. **Katixa Lajaunie-Salla:** Writing - review & editing. **Pierre Marrec:** Writing - review & editing. **Thibaut Wagener:** Conceptualization, Investigation, Visualization, Writing - review & editing, Supervision. **Patrick Raimbault:** Investigation, Writing - review & editing, Supervision. **Véronique Lagadec:** Investigation, Formal analysis. **Michel Lafont:** Resources, Investigation. **Nicole Garcia:** Investigation, Formal analysis. **Frédéric Diaz:** Writing - review & editing. **Christel Pinazo:** Writing - review & editing. **Christophe Yohia:** Software, Investigation, Formal analysis. **Fabrice Garcia:** Investigation, Formal analysis. **Irène Xueref-Remy:** Writing - review & editing, Validation, Investigation, Formal analysis. **Pierre-Eric Blanc:** Investigation. **Alexandre Armengaud:** Validation, Investigation, Formal analysis. **Dominique Lefèvre:** Conceptualization, Writing - review & editing, Investigation, Supervision.

Declaration of competing interests

The authors declare that they have no known competing financial interests or personal relationships that could have appeared to influence the work reported in this paper.

Acknowledgements

We thank the Service d'Observation en MILieu Littoral (SOMLIT) for its permission to use SOLEMIO data. We wish to thank the crewmembers of the R.V. 'Antedon II', operated by the DT-INSU, for making these samplings possible. We wish to acknowledge the team of the SAM platform (Service ATmosphère et océan) for their helping in field work. For seawater sample analyses, we also thank the SNAPO-CO_2 at LOCEAN, Paris. The SNAPO-CO_2 service at LOCEAN is supported by CNRS-INSU and OSU Ecce-Terra. Some additional data has been obtained from the MOOSE data base (http://mistrals.sedoo.fr/MOOSE/). We acknowledge the https://www.infoclimat.fr for providing the Météo-France station data. We thank the two anonymous reviewers for their helpful comments to improve this paper.

Appendix A. Supplementary data

Supplementary data to this article can be found online at https://doi.org/10.1016/j.ecss.2020.106641.

References

Álvarez, M., Sanleón-Bartolomé, H., Tanhua, T., Mintrop, L., Luchetta, A., Cantoni, C., Schroeder, K., Civitarese, G., 2014. The CO_2 system in the Mediterranean Sea: a basin wide perspective. Ocean Sci. 10 (1), 69–92. doi:10.5194/os-10-69-2014.

Aminot, A., Kérouel, R., 2007. Dosage automatique des nutriments dans les eaux marines: méthodes en flux continu. Editions Ifremer.

Astor, Y.M., Lorenzoni, L., Thunell, R., Varela, R., Muller-Karger, F., Troccoli, L., Taylor, G.T., Scranton, M.I., Tappa, E., Rueda, D., 2013. Interannual variability in sea surface temperature and fCO_2 changes in the Cariaco Basin. Deep Sea Res. Part II 93, 33–43. doi:10.1016/j.dsr2.2013.01.002.

Bensoussan, N., Gattuso, J.-P., 2007. Community primary production and calcification in a NW Mediterranean ecosystem dominated by calcareous macroalgae. Mar. Ecol. Prog. Ser. 334, 37–45. doi:10.3354/meps334037.

Borges, A.V., Schiettecatte, L.-S., Abril, G., Delille, B., Gazeau, F., 2006. Carbon dioxide in European coastal waters. Estuar. Coast Shelf Sci. 70 (3), 375–387. doi:10.1016/j.ecss.2006.05.046.

Borges, A.V., Ruddick, K., Schiettecatte, L.-S., Delille, B., 2008. Net ecosystem production and carbon dioxide fluxes in the Scheldt estuarine plume. BMC Ecol. 8 (15). 0-15. doi:10.1186/1472-6785-8-15.

Bourgeois, T., Orr, J.C., Resplandy, L., Terhaar, J., Ethé, C., Gehlen, M., Bopp, L., 2016. Coastal-ocean uptake of anthropogenic carbon. Biogeosciences 13 (14), 4167–4185. doi:10.5194/bg-13-4167-2016.

De Carlo, E.H., Mousseau, L., Passafiume, O., Drupp, P.S., Gattuso, J.-P., 2013. Carbonate chemistry and air–sea CO_2 flux in a NW Mediterranean Bay over a four-year period: 2007–2011. Aquat. Geochem. 19 (5–6), 399–442. doi:10.1007/s10498-013-9217-4.

Carstensen, J., Duarte, C.M., 2019. Drivers of pH variability in coastal ecosystems. Environ. Sci. Technol. 53 (8), 4020–4029. doi:10.1021/acs.est.8b03655.

Clayton, T.D., Byrne, R.H., 1993. Spectrophotometric seawater pH measurements: total hydrogen ion concentration scale calibration of m-Cresol purple and at-Sea results. Deep Sea Res. Oceanogr. Res. Pap. 40 (10), 2115–2129. doi:10.1016/0967-0637(93)90048-8.

Copin-Montégut, C., 1993. Alkalinity and carbon budgets in the Mediterranean Sea. Global Biogeochem. Cycles 7 (4), 915–925. doi:10.1029/93GB01826.

Copin-Montégut, C., Bégovic, M., 2002. Distributions of carbonate properties and oxygen along the water column (0–2000m) in the central part of the NW Mediterranean Sea (Dyfamed Site): influence of winter vertical mixing on air–sea CO_2 and O_2 exchanges. Deep Sea Res. Part II Top. Stud. Oceanogr. 49 (11), 2049–2066. doi:10.1016/S0967-0645(02)00027-9.

Copin-Montégut, C., Bégovic, M., Merlivat, L., 2004. Variability of the partial pressure of CO_2 on diel to annual time scales in the Northwestern Mediterranean Sea. Mar. Chem. 85 (3–4), 169–189. doi:10.1016/j.marchem.2003.10.005.

Coppola, L., Diamond Riquier, E., Carval, T., 2018. Dyfamed Observatory Data. SEANOE. doi:10.17882/43749.

Courtney, T.A., Andersson, A.J., 2019. Evaluating measurements of coral reef net ecosystem calcification rates. Coral Reefs 38 (5), 997–1006. https://doi:10.1007/s00338-019-01828-2.

Dean, J.A., Lange, N.A. (Eds.), 1999. Lange's Handbook of Chemistry, 15 ed. McGraw-Hill Handbooks, New York, NY: McGraw-Hill.

Diaz, F., Naudin, J.-J., Courties, C., Rimmelin, P., Oriol, L., 2008. Biogeochemical and ecological functioning of the low-salinity water lenses in the region of the Rhone River freshwater influence, NW Mediterranean Sea. Continent. Shelf Res. 28 (12), 1511–1526. https://doi/10.1016/j.csr.2007.08.009.

Dickson, A.G., 1990. Standard potential of the reaction: AgCl(s) + 1/2 H_2(g) = Ag(s) + HCl(aq), and the standard acidity constant of the ion HSO_4^- in synthetic sea water from 273.15 to 318.15 K. J. Chem. Therm. 22 (2), 113–127. doi:10.1016/0021-9614(90)90074-Z.

Dickson, A.G., Sabine, C.L., Christian, J.R., Bargeron, C.P., North Pacific Marine Science Organization (Eds.), 2007. Guide to Best Practices for Ocean CO2 Measurements, 3. PICES Special Publication, Sidney, BC. North Pacific Marine Science Organization.

Dickson, A.G., Goyet, C. (Eds.), 1994. Handbook of Methods for the Analysis of the Various Parameters of the Carbon Dioxide System in Sea Water. Version 2, no 74, US Department of Energy.

Dickson, A.G., Millero, F., 1987. A comparison of the equilibrium constants for the dissociation of carbonic acid in seawater media. Deep Sea Res. 34 (10), 1733–1743. doi:10.1016/0198-0149(87)90021-5.

Dlugokencky, E., Tans, P., 2019. Trends in Atmospheric Carbon Dioxide. National Oceanic & Atmospheric Administration, Earth System Research Laboratory (NOAA/ESRL). available at:. http://www.esrl.noaa.gov/gmd/ccgg/trends/global.html (last access: November 23th 2018).

Doney, S.C., Fabry, V.J., Feely, R.A., Kleypas, J.A., 2009. Ocean acidification: the other CO_2 problem. Ann. Rev. Mar. Sci. 1 (1), 169–192. https://doi/10.1146/annurev.marine.010908.163834.

Durrieu de Madron, X., Guieu, C., Sempéré, R., Conan, P., Cossa, D., D'Ortenzio, F., Estournel, C., Gazeau, F., Rabouille, C., Stemmann, L., Bonnet, S., Diaz, F., Koubbi, P., Radakovitch, O., Babin, M., Baklouti, M., Bancon-Montigny, C., Belviso, S., Bensoussan, N., Bonsang, B., Bouloubassi, I., Brunet, C., Cadiou, J.-F., Carlotti, F., Chami, M., Charmasson, S., Charrière, B., Dachs, J., Doxaran, D., Dutay, J.-C., Elbaz-Poulichet, F., Eléaume, M., Eyrolles, F., Fernandez, C., Fowler, S., Francour, P., Gaertner, J.C., Galzin, R., Gasparini, S., Ghiglione, J.-F., Gonzalez, J.-L., Goyet, C., Guidi, L., Guizien, K., Heimbürger, L.-E., Jacquet, S.H.M., Jeffrey, W.H., Joux, F., Le Hir, P., Leblanc, K., Lefèvre, D., Lejeusne, C., Lemé, R., Loÿe-Pilot, M.-D., Mallet, M., Méjanelle, L., Mélin, F., Mellon, C., Mérigot, B., Merle, P.-L., Migon, C., Miller, W.L., Mortier, L., Mostajir, B., Mousseau, L., Moutin, T., Para, J., Pérez, T., Petrenko, A., Poggiale, J.-C., Prieur, L., Pujo-Pay, M., Pulido-Villena, E., Raimbault, P., Rees, A.P., Ridame, C., Rontani, J.-F., Ruiz Pino, D., Sicre, M.A., Taillandier, V., Tamburini, C., Tanaka, T., Taupier-Letage, I., Tedetti, M., Testor, P., Thébault, H., Thouvenin, B., Touratier, F., Tronczynski, J., Ulses, C., Van Wambeke, F., Vantrepotte, V., Vaz, S., Verney, R., 2011. Marine ecosystems' responses to climatic and anthropogenic forcings in the Mediterranean. Prog. Oceanogr. 91 (2), 97–166. doi:10.1016/j.pocean.2011.02.003.

Edmond, J.M., 1970. High precision determination of titration alkalinity and total carbon dioxide content of sea water by potentiometric titration. Deep-Sea Res. Oceanogr. Abstr. 17 (4), 737–750. doi:10.1016/0011-7471(70)90038-0.

Fraysse, M., Pairaud, I., Ross, O.N., Faure, V.M., Pinazo, C., 2014. Intrusion of Rhone river diluted water into the Bay of Marseille: generation processes and impacts on ecosystem functioning. J. Geophys. Res.: Oceans 119 (10), 6535–6556. doi:10.1002/2014JC010022.

Gangloff, A., Verney, R., Doxaran, D., Ody, A., Estournel, C., 2017. Investigating rhône River plume (gulf of Lions, France) dynamics using metrics analysis from the MERIS 300m ocean color archive (2002–2012). Continent. Shelf Res. 144, 98–111. doi:10.1016/j.csr.2017.06.024.

Gatti, J., Petrenko, A., Devenon, J.-L., Leredde, Y., Ulses, C., 2006. The Rhone River dilution zone present in the north eastern shelf of the gulf of lion in december 2003. Continent. Shelf Res. 26 (15), 1794–1805. doi:10.1016/j.csr.2006.05.012.

Gattuso, J.-P., Frankignoulle, M., Wollast, R., 1998. Carbon and carbonate metabolism in coastal aquatic ecosystems. Annu. Rev. Ecol. Systemat. 29 (1), 405–434. doi:10.1146/annurev.ecolsys.29.1.405.

Gazeau, F., Duarte, C.M., Gattuso, J.-P., Barrón, C., Navarro, N., Ruíz, S., Prairie, Y.T., Calleja, M., Delille, B., Frankignoulle, M., Borges, A.V., 2004. Whole-system metabolism and CO_2 fluxes in a mediterranean bay dominated by seagrass beds (Palma bay, NW mediterranean). Biogeosci. Discuss. 1 (1), 755–802. doi:10.5194/bgd-1-755-2004.

Gruber, N., Clement, D., Carter, B.R., Feely, R.A., Van Heuven, S., Hoppema, M., Ishii, M., Key, R.M., Kozyr, A., Lauvset, S.K., Lo Monaco, C., Mathis, J.T., Murata, A., Olsen, A., Perez, F.F., Sabine, C.L., Tanhua, T., Wanninkhof, R., 2019. The oceanic sink for anthropogenic CO_2 from 1994 to 2007. Science 363 (6432), 1193–1199. doi:10.1126/science.aau5153.

Hassoun, A.E.R., Gemayel, E., Krasakopoulou, E., Goyet, C., Saab, M.A.-A., Ziveri, P., Touratier, F., Guglielmi, V., Falco, C., 2015. Modeling of the total alkalinity and the total inorganic carbon in the Mediterranean Sea. J. Water Resour. Ocean Sci. 4 (1), 24. doi:10.11648/j.wros.20150401.14.

Ho, D.T., Law, C.S., Smith, M.J., Schlosser, P., Harvey, M., Hill, P., 2006. Measurements of air-sea gas exchange at high wind speeds in the Southern Ocean: implications for global parameterizations. Geophys. Res. Lett. 33 (16). doi:10.1029/2006GL026817.

Hood, E.M., Merlivat, L., 2001. Annual to interannual variations of CO_2 in the Northwestern Mediterranean Sea: results from hourly measurements made by CARIOCA buoys, 1995-1997. J. Mar. Res. 59 (1), 113–131. doi:10.1357/002224001321237399.

Huang, Y.-H., Lee, C.-L., Chung, C.-Y., H, S.-C., Lin, H.-J., 2015. Carbon budgets of multispecies seagrass beds at dongsha Island in the South China sea. Mar. Environ. Res. 106 (1), 92–102. doi:10.1016/j.marenvres.2015.03.004.

Hunt, C.W., Salisbury, J.E., Vandemark, D., 2011. Contribution of non-carbonate anions to total alkalinity and overestimation of pCO_2 in New England and New Brunswick rivers. Biogeosciences 8 (10), 3069–3076. 2011. doi:10.5194/bg-8-3069-2011.

Ingrosso, G., Giani, M., Comici, C., Kralj, M., Piacentino, S., De Vittor, C., Del Negro, P., 2016. Drivers of the carboante system seasonal variations in a Mediterranean gulf. *Estuarine*. Coast. Shelf Sci. 168, 58–70. doi:10.1016/j.ecss.2015.11.001.

IPCC, 2018. Summary for policymakers. In: Masson-Delmotte, V., Zhai, P., Pörtner, H.-O., Roberts, D., Skea, J., Shukla, P.R., Pirani, A., Moufouma-Okia, Péan, C., Pidcock, R., Connors, S., Matthews, J.B.R., Chen, Y., Zhou, X., Gomis, M.I., Lonnoy, E., Maycock, Tignor, M., Waterfield, T. (Eds.), Global Warming of 1.5°C. An IPCC Special Report on the Impacts of Global Warming of 1.5°C above Pre-industrial Levels and Related Global Greenhouse Gas Emission Pathways, in the Context of Strengthening the Global Response to the Threat of Climate Change, Sustainable Development, and Efforts to Eradicate Poverty. World Meteorological Organization, Geneva, Switzerland, p. 32.

Kapsenberg, L., Alliouane, S., Gazeau, F., Mousseau, L., Gattuso, J.-P., 2017. Coastal ocean acidification and increasing total alkalinity in the Northwestern Mediterranean Sea. Ocean Sci. 13 (3), 411–426. doi:10.5194/os-13-411-2017.

Kirchman, D.L., 2000. Uptake and regeneration of inorganic nutrients by marine heterotrophic bactiria. In: Kirchman, D.L. (Ed.), Microbial Ecology of the Oceans. Wiley, pp. 261–288.

Kirkman, H., Reid, D.D., 1979. A study of the role of the seagrass *Posidonia australis* in the carbon budget of an estuary. Aquat. Bot. 7, 173–183. doi:10.1016/0304-3770(79)90020-2.

Laruelle, G.G., Lauerwald, R., Pfeil, B., Regnier, P., 2014. Regionalized global budget of the CO_2 exchange at the air-water interface in continental shelf seas. Global Biogeochem. Cycles 28 (11), 1199–1214. doi:10.1002/2014GB004832.

Lefèvre, D., 2010. MOOSE (ANTARES). doi:10.18142/233.

Louanchi, F., Boudjakdji, M., Nacef, L., 2009. Decadal changes in surface carbon dioxide and related variables in the Mediterranean Sea as inferred from a coupled data-diagnostic model approach. ICES (Int. Counc. Explor. Sea) J. Mar. Sci. 66 (7), 1538–1546. doi:10.1093/icesjms/fsp049.

Meeder, E., Mackey, K.R.M., Paytan, A., Shaked, Y., Iluz, D., Stambler, N., Rivlin, T., Post, A.F., Lazar, B., 2012. Nitrite dynamics in the open ocean - clues from seasonal and diurnal variations. Mar. Ecol. Prog. Ser. 453, 11–26. doi:10.3354/meps09525.

Mehrbach, C., Culberson, C.H., Hawley, J.E., Pytkowicz, R.M., 1973. Measurement of the apparent dissociation constants of carbonic acid in seawater at atmospheric pressure. Limnol. Oceanogr. 18 (6), 897–907. doi:10.4319/lo.1973.18.6.0897.

Merlivat, L., Boutin, J., Antoine, D., Beaumont, L., Golbol, M., Vellucci, V., 2018. Increase of dissolved inorganic carbon and decrease in pH in near-surface waters in the Mediterranean Sea during the past two decades. Biogeosciences 15 (18), 5653–5662. doi:10.5194/bg-15-5653-2018.

Millero, F.J., 1995. Thermodynamics of the carbon dioxide system in the oceans. Geochem. Cosmochim. Acta 59 (4), 661–677. doi:10.1016/0016-7037(94)00354-O.

Millero, F.J., Lee, K., Roche, M., 1998. Distribution of alkalinity in the surface waters of the major oceans. Mar. Chem. 60 (1–2), 111–130. doi:10.1016/S0304-4203(97)00084-4.

Millet, B., Pinazo, C., Banaru, D., Pagès, R., Guiart, P., Pairaud, I., 2018. Unexpected spatial impact of treatment plant discharges induced by episodic hydrodynamic events: modelling Lagrangian transport of fine particles by Northern Current intrusions in the Bays of Marseille (France). Édité par João Miguel Dias. PloS One 13 (4), e0195257. doi:10.1371/journal.pone.0195257.

Monterey, G., Levitus, S., 1997. In: Seasonal Variability of Mixed Layer Depth for the World Ocean. NOAA Atlas NESDIS, 14. U. S. Govt. Printing Office.

Nykjaer, L., 2009. Mediterranean Sea surface warming 1985-2006. Clim. Res. 39 (1), 11–17. doi:10.3354/cr00794.

Olafsson, J., Olafsdottir, S.R., Benoit-Cattin, A., Takahashi, T., 2010. The Irminger Sea and the Iceland Sea time series measurements of sea water carbon and nutrient chemistry 1983–2008. Earth Syst. Sci. Data 2 (1), 99–104. doi:10.5194/essd-2-99-2010.

Oudot, C., 1989. O_2 and CO_2 balances approach for estimating production in the mixed layer of the tropical Atlantic Ocean (Guinea Dome area). J. Mar. Res. 47, 385–409.

Petrenko, A., 2003. Variability of circulation features in the gulf of lion NW Mediterranean Sea. Importance of inertial currents. Oceanol. Acta 26 (4), 323–338. doi:10.1016/S0399-1784(03)00038-0.

Pierrot, D., Lewis, E., Wallace, D.W.R., 2006. MS Excel Program Developed for CO_2 System Calculations, Tech. rep., Carbon Dioxide Inf. Anal. Cent.. Oak Ridge Natl. Lab., US DOE, Oak Ridge, Tenn.

Pont, D., Simonnet, J.-P., Walter, A.V., 2002. Medium-term changes in suspended sediment delivery to the ocean: consequences of catchment heterogeneity and river management (Rhone river, France). *Estuarine*. Coast. Shelf Sci. 54 (1), 1–18. doi:10.1006/ecss.2001.0829.

Rivaro, P., Messa, R., Massolo, S., Frache, R., 2010. Distributions of carbonate properties along the water column in the Mediterranean Sea: spatial and temporal variations. Mar. Chem. 121 (1–4), 236–245. doi:10.1016/j.marchem.2010.05.003.

Schneider, A., Wallace, D.W.R., Körtzinger, A., 2007. Alkalinity of the Mediterranean Sea: alkalinity of the Mediterranean Sea. Geophys. Res. Lett. 34 (15), L15608. doi:10.1029/2006GL028842.

Soetaert, K., Hofmann, A.F., Middelburg, J.J., Meysman, F.J.R., Greenwood, J., 2007. The effect of biogeochemical processes on pH. Mar. Chem. 105 (1), 30–51. doi:10.1016/j.marchem.2006.12.01.

Sokal, R.R., Rohlf, F.J., 1969. Biometry. The Principles and Practices of Statistics in Biological Research. second ed. W.H. Freeman, San Francisco.

Suzuki, A., Kawahata, H., 2003. Carbon budget of coral reef systems: an overview of observations in fringing reefs, barrier reefs and atolls in the Indo-Pacific regions. Tellus B 55 (2), 428–444. doi:10.1034/j.1600-0889.2003.01442.x.

Sverdrup, H.U., 1953. On conditions for the vernal blooming of phytoplankton. ICES (Int. Counc. Explor. Sea) J. Mar. Sci. 18 (3), 287–295. doi:10.1093/icesjms/18.3.287.

Taillandier, V., D'Ortenzio, F., Antoine, D., 2012. Carbon fluxes in the mixed layer of the Mediterranean Sea in the 1980s and the 2000s. Deep Sea Res. Oceanogr. Res. Pap. 65, 73–84. doi:10.1016/j.dsr.2012.03.004.

Takahashi, T., Olafsson, J., Goddard, J.G., Chipman, D.W., Sutherland, S.C., 1993. Seasonal variation of CO2 and nutrients in the high-latitude surface oceans: a comparative study. Global Biogeochem. Cycles 7 (4), 843–878. doi:10.1029/93GB02263.

Takahashi, T., Sutherland, S.C., Sweeney, C., Poisson, A., Metzl, N., Tilbrook, B., Bates, N., Wanninkhof, R., Feely, R.A., Sabine, C., Olafsson, J., Nojiri, Y., 2002. Global sea–air CO_2 flux based on climatological surface ocean pCO_2, and seasonal biological and temperature effects. Deep Sea Res. Part II Top. Stud. Oceanogr. 49 (9–10), 1601–1622. doi:10.1016/S0967-0645(02)00003-6.

Touratier, F., Goyet, C., 2009. Decadal evolution of anthropogenic CO_2 in the north western Mediterranean Sea from the mid-1990s to the mid-2000s. Deep Sea Res. Part I 56 (10), 1708–1716. doi:10.1016/j.dsr.2009.05.015.

Vargas-Yáñez, M., Garciá, J., Salat, J., Garciá-Marti, M.C., Pascual, J., Moya, F., 2008. Warming trends and decadal variability in the Western Mediterranean shelf. Global Planet. Change 63 (2–3), 177–184. doi:10.1016/j.gloplacha.2007.09.001.

Wanninkhof, R., 2014. Relationship between wind speed and gas exchange over the ocean revisited. Limnol Oceanogr. Methods 12 (6), 351–362. doi:10.4319/lom.2014.12.351.

Wanninkhof, R., McGillis, W.R., 1999. A cubic relationship between air-Sea CO_2 exchange and wind speed. Geophys. Res. Lett. 26 (13), 1889–1892. doi:10.1029/1999GL900363.

Wanninkhof, R., Park, G.H., Takahashi, T., Sweeney, C., Feely, R., Nojiri, Y., Gruber, N., Doney, S.C., McLinley, G.A., Lenton, A., Le Quéré, C., Heinze, C., Schwinger, J., Graven, H., Khatiwala, S., 2013. Global ocean carbon uptake: magnitude, variability and trends. Biogeosciences 10 (3), 1983–2000.

Ward, B., 1985. Light and substrate concentration relationships with marine ammonium assimilation and oxidation rates. Mar. Chem. 16 (4), 301–316. doi:10.1016/0304-4203(85)90052-0.

Ware, J.R., Smith, S.V., Reaka-Kudla, M.L., 1992. Coral reefs: sources or sinks of atmospheric CO_2? Coral Reefs 11 (3), 127–130. doi:10.1007/BF00255465.

Weiss, R.F., 1974. Carbon dioxide in water and seawater: the solubility of a non-ideal gas. Mar. Chem. 2 (3), 203–215. doi:10.1016/0304-4203(74)90015-2.

Wolf-Gladrow, D.A., Zeebe, R.E., Klaas, C., Körtzinger, A., Dickson, A.G., 2007. Total alkalinity: the explicit conservative expression and its application to biogeochemical processes. Mar. Chem. 106 (1–2), 287–300. doi:10.1016/j.marchem.2007.01.006.

Wollast, R., 1998. Evaluation and comparison of the global carbon cycle in the coastal zone and in the open ocean. In: Brink, K.H., Robinson, A.R. (Eds.), The Sea. John Wiley & Sons, New York, pp. 213–252.

Xueref-Remy, I., Dieudonné, E., Vuillemin, C., Lopez, M., Lac, C., Schmidt, M., Delmotte, M., Chevallier, F., Ravetta, F., Perrussel, O., Ciais, P., Bréon, F.-M., Broquet, G., Ramonet, M., Spain, T.G., Ampe, C., 2018. Diurnal, synoptic and seasonal variability of atmospheric CO2 in the Paris megacity area. Atmos. Chem. Phys. 18 (5), 3335–3362. doi:10.5194/acp-18-3335-2018.

Yao, W., Liu, X., Byrne, R.H., 2007. Impurities in indicators used for spectrophotometric seawater pH measurements: assessment and remedies. Mar. Chem. 107 (2), 167–172. doi:10.1016/j.marchem.2007.06.012.

Zakem, E.J., Al-Haj, A., Church, M.J., Van Dijken, G.L., Dutkiewicz, S., Foster, S.Q., Fulweiler, R.W., Mills, M.M., Folows, M.J., 2018. Ecological control of nitrite in the upper ocean. Nat. Commun. 9 (1206), 1–13. doi:10.1038/s41467-018-03553-w.